

# L1PP PERFORMANCE ANALYSIS FOR SMOS IN ORBIT COMMISSIONING PHASE

Rita Castro<sup>(1)</sup>, Roger Oliva<sup>(2)</sup>, Jose Barbosa<sup>(3)</sup>, Antonio Gutierrez<sup>(4)</sup>, Sofia Freitas<sup>(5)</sup>, Eric Anterrieu<sup>(6)</sup>, Adriano Camps<sup>(7)</sup>, Manuel Martin-Neira<sup>(8)</sup> and Michele Zundo<sup>(9)</sup>

<sup>(1)</sup>Deimos Engenharia - Aerospace Systems, Av. D. João II, Lote 1.17 Torre Zen, 10º, 1998-023 Lisboa (PORTUGAL),  
Email: [rita.castro@deimos.com.pt](mailto:rita.castro@deimos.com.pt)

<sup>(2)</sup>ESA, European Space Research & Technology Centre Keplerlaan 1 - Postbus 299 - 2200 AG Noordwijk  
(NETHERLANDS), Email: [roger.oliva.balague@esa.int](mailto:roger.oliva.balague@esa.int)

<sup>(3)</sup>Deimos Engenharia - Aerospace Systems, Av. D. João II, Lote 1.17 Torre Zen, 10º, 1998-023 Lisboa (PORTUGAL),  
Email: [jose.barbosa@deimos.com.pt](mailto:jose.barbosa@deimos.com.pt)

<sup>(4)</sup>Deimos Engenharia - Aerospace Systems, Av. D. João II, Lote 1.17 Torre Zen, 10º, 1998-023 Lisboa (PORTUGAL),  
Email: [antonio.gutierrez@deimos.com.pt](mailto:antonio.gutierrez@deimos.com.pt)

<sup>(5)</sup>Deimos Engenharia - Aerospace Systems, Av. D. João II, Lote 1.17 Torre Zen, 10º, 1998-023 Lisboa (PORTUGAL),  
Email: [sofia.freitas@deimos.com.pt](mailto:sofia.freitas@deimos.com.pt)

<sup>(6)</sup>Observatoire Midi-Pyrénées – Laboratoire d’Astrophysique, UMR5572 - 14 av. Edouard Belin 31400 Toulouse  
(FRANCE), Email: [eric.anterrieu@ast.obs-mip.fr](mailto:eric.anterrieu@ast.obs-mip.fr)

<sup>(7)</sup>Universitat Politècnica de Catalunya – Signal Theory and Communications Department, Campus Nord UPC Office  
D4-016 C/Jordi Girona 1-3 08034 Barcelona (SPAIN), Email: [camps@tsc.upc.edu](mailto:camps@tsc.upc.edu)

<sup>(8)</sup>ESA, European Space Research & Technology Centre Keplerlaan 1 - Postbus 299 - 2200 AG Noordwijk  
(NETHERLANDS), Email: [manuel.martin-neira@esa.int](mailto:manuel.martin-neira@esa.int)

<sup>(9)</sup>ESA, European Space Research & Technology Centre Keplerlaan 1 - Postbus 299 - 2200 AG Noordwijk  
(NETHERLANDS), Email: [michele.zundo@esa.int](mailto:michele.zundo@esa.int)

## ABSTRACT

Following SMOS launch in November 2009, a Commissioning Phase has taken place for six months, having Deimos closely cooperated with Level 1 ESA team. During these six months several studies have been conducted on calibration optimization, image reconstruction improvement, geolocation assessment and the impact on scientific results, in particular to ensure optimal input to Level 2 Soil Moisture and Ocean Salinity retrieval.

Some of the new features in the Level 1 processing chain that have been studied during Commissioning include:

- Calibration routines, where new algorithms have been tested for the first time (calibration of PMS-values using the Cold Sky as a reference target) and others have been fine-tuned (the Local Oscillator calibration frequency);
- Foreign Sources Mitigation algorithms have been checked and validated with real data;
- Geolocated data has been analysed and the retrieved scientific results (pixel bias, scene bias, etc) are within the limits expected by Level 2 Teams.

Deimos and ESA have also defined and implemented the requirements for the operational Auxiliary Data Files (ADFs), namely the System Response Function (G-matrix), its Pseudo-Inverse ( $J^+$ -Matrix) [6] and the

Flat Target Response [4]. The System Response Function Pseudo-Inverse is the responsible for transforming the visibilities coming from the instrument to brightness temperatures and the Flat Target Response corrects the systematic errors caused by errors in the Antenna Patterns measurements.

Deimos and ESA will report on the main results achieved and present the final Level 1 processing performance achieved at the end of the Commissioning Phase. This shall comprise:

- Impact on the L1c Brightness Temperature of:
  - Local Oscillator calibration frequency;
  - Different Foreign Sources Algorithms configurations e.g. direct Sky and Moon, Sun glint and backlobes contribution);
- Instrument accuracy obtained using the Galaxy as a target;
- Final assessment on Dual Polarisation versus Full Polarisation data.

## 1. INTRODUCTION

This section presents a synthetic description of the processing chain for the Level 1 of SMOS, in particular, the architecture of the Prototype Processor. A brief summary of the notation used in this paper is also presented in this paper.

For more details on processing Level 1 data, please refer to [1], [7] and [8].

## 1.1. Overview of the Level 1 Processor Prototype

The Level 1 Processor Prototype (L1PP) for the SMOS mission is a software processing chain that will convert all satellite data from raw products (L0 data) into geolocated measured brightness temperatures at different observation angles (L1c data). It was built to be used as a test bed for the SMOS processing algorithms and product definitions and as such it has to be a flexible tool that enables fast implementation and testing of different scenarios (algorithms, instrument behavior, data availability, data corruption, etc.). L1PP was extensively used during the Commissioning Phase to verify the algorithms and calibration strategies.

The data processing is divided into three main steps: calibration, image reconstruction and geolocation. Each of these steps will generate data products that are used to store relevant intermediate information. These steps are:

- Level 0 digital counts to Calibrated Visibilities (Level 1a);
- Image reconstruction i.e. Calibrated Visibilities to Brightness temperatures (Level 1b);
- Brightness temperature in the instrument frame to geolocated map (Level 1c).

The existence of this clear division between each set of algorithms increases modularity and the intermediate products (L1a and L1b) enables the processor to use a database of calibration data. They are further divided into separate processing units that are designed to implement self-contained sets of processing algorithms.

The L0 to L1a processing units are:

- Unit Converter – makes the conversion of ancillary data (HKTm) into engineering units;
- Raw correlations and Autocalibration modules – convert digital correlator counts into quadrature corrected correlations;
- Correlated and Uncorrelated Noise Injection modules – derive in-orbit calibration coefficients from correlated and uncorrelated noise injection sequences;
- Noise Injection Radiometer (NIR) calibration module – computes the NIR calibration parameters;
- Error correction module – applies calibration data to quadrature corrected visibilities and computes Calibrated Visibilities.

In L1a to L1b we have:

- Image Reconstruction Module – computes the brightness temperatures for each snapshot;
- Foreign Sources Correction – removes brightness temperature contributions from external sources.

And in L1b to L1c processing there is a single processing unit to geolocate the brightness temperatures

and construct half-orbit swaths with a set of observations at different angles for each pixel.

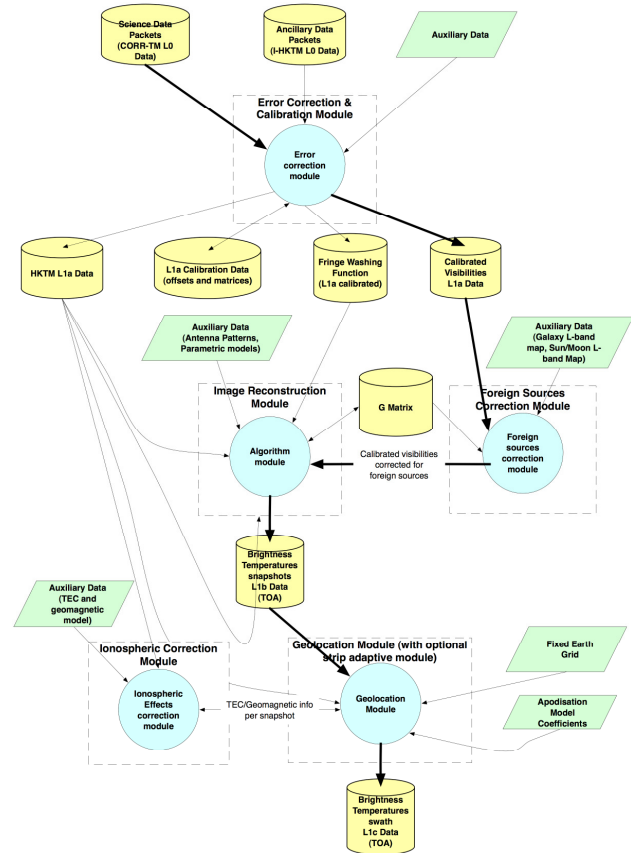


Figure 1. L1PP Module decomposition and data flow

## 1.2. Notation

In this paper we will use the following notation to describe data acquired with MIRAS:

- *Dual Polarization Scene(s)*: corresponds to data acquired with the instrument in DUAL polarimetric mode. In this mode there are two possible polarizations (H and V)
- *Full Polarization Scene(s)*: corresponds to data acquired with the instrument in FULL polarimetric mode. There are three possible polarizations: H, V and HV and the first two can be divided in two sub-types:
  - *Pure Scene*: corresponds to a snapshot acquired by MIRAS when all the three arms are in the same polarization during an epoch, i.e., 1.2 seconds.
  - *Mixed Scene*: corresponds to a snapshot obtained during an epoch, i.e., 1.2 seconds, in which MIRAS has its arms changing their polarization modes each  $1.2/3 = 0.4$  seconds.

## 2. LOCAL OSCILLATOR CALIBRATION FREQUENCY

The Local Oscillator (LO) calibration of the MIRAS instrument is essential for the tracking of the Fringe Washing-Function (FWF) phase. This phase was found to be particularly dependent on orbital temperature variations during on-ground tests. Thus, a regular sampling of this phase became necessary in order to properly calibrate the measurements. During the SMOS commissioning phase, a study was made in order to determine the optimal sampling frequency that would provide optimal quality data while reducing the measurement losses due to calibration activities [12]. The specific objectives were:

- To do an analysis of the LO rate needed in order to correctly track the phase behavior (by estimating the error committed at a rate of every minute compared to 2-16 min);
- To study the effects of the Local Oscillator calibration frequency in the reconstructed Brightness Temperatures;
- To give L2 teams recommendations from L1 point of view for the calibration frequency necessary to cope with SMOS requirements, in terms of data quality and observation time.

A mechanism to decimate the LO calibration sequences was implemented in LIPP, in order to be able to use data acquired with a constant rate of 1 minute to study the effect of each inter-calibration period.

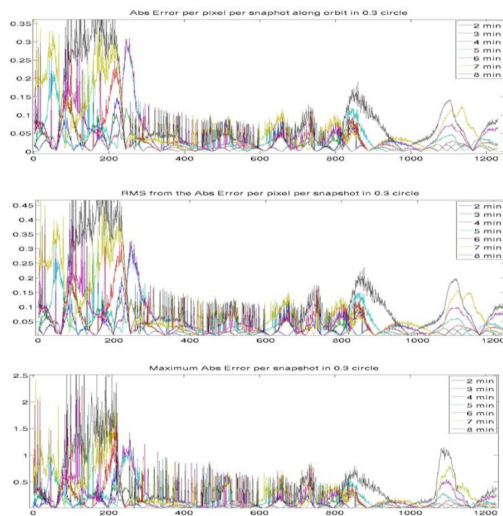


Figure 2. Absolute Error (top), Spatial RMS of Error (middle) and Maximum Error for the  $(\xi, \eta)$  points inside the Circle  $r=0.3$ (bottom) (H-pol)

In Fig.2, the errors in reconstructed Brightness Temperature are plotted against LO frequency for a sample orbit in H-pol. This exercise was made for several orbits and all polarization modes and the results are shown in Fig.3.

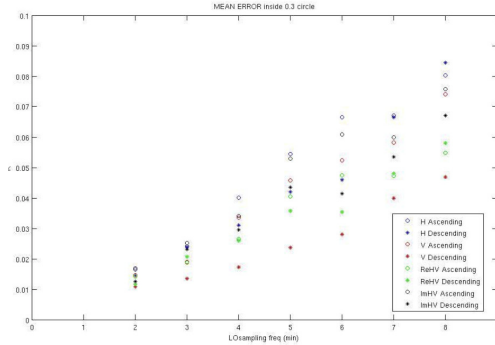


Figure 3. Mean Error tables for the same orbit in all polarizations

In these plots it becomes clear that V polarization is less perturbed than H polarization. Since there is no special reason to favor V, the difference must come from the phase problems linked to a particular receiver, in this case the NIR-AB in H-pol, which affected only this polarization data. In all cases, a linear increasing trend of the errors with respect to the sampling frequency is observed. The differences between Ascending and Descending depend more on the specific orbit being studied than in any particular characteristic of the pass itself. Having the sampling points on certain transitions can improve the results. For this reason the full study was based on several orbits, in order to improve its statistical significance.

As for the effect of NIR-AB in H-pol, another study was performed to analyze its behavior. Using data from a different orbit, a comparison was made between the 4, 6 and 8 minutes interpolation based on 2 minutes sampling, compared to the same data (to 4 minutes only) when all the baselines involving NIR-AB in H-pol were removed from the image reconstructed.

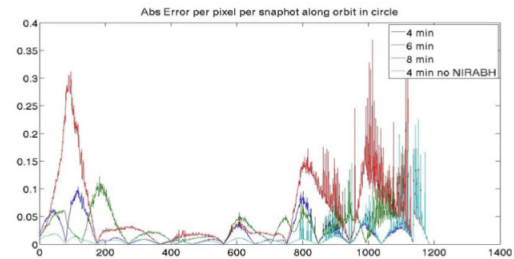


Figure 4. Absolute error for all baselines excluding the ones involving NIR AB H (H-pol)

The maximum absolute error was now at the level of the results obtained for V-pol. The conclusion was that a specific algorithm must be used to track phase of NIR-AB in H-pol, since that particular receiver was being affected by a nearby heating system, or that the baselines involving this receiver should be removed from the reconstruction.

A subsequent study performed by the L2 team excluded the option to remove the NIR-AB in H-pol baselines and an alternate method for phase tracking of this receiver is being investigated by Deimos Engenharia and ESA.

## 2.1. Summary

The final conclusions of this study were:

- The error introduced by using an interval of LO calibration smaller than 5 minutes is very small in terms of Phase tracking and do not exceed a threshold of 3 degrees in 99.7% of the time (excluding the NIR-AB in H-pol baseline).
- By analyzing the impact on to Brightness Temperature there is a linear increase of the error with the spacing of the local oscillator calibration.

The inputs from this study were passed to the SMOS management board, which allowed them to reach a final agreement to sample the Local Oscillator phase every 10 minutes.

## 3. FOREIGN SOURCES ALGORITHMS EVALUATION

The L1PP was used to test the efficiency of several algorithms designed to eliminate the contribution of known Foreign Sources from the reconstruction process, like the Sun, Moon and Galaxy direct radiation (allowing the extension of the alias free field of view [2]), the Sun radiation reflected on the sea surface (Sun glint) and the amount of radiation received through the backlobes of the antennas as well as the Corbella term [10].

In order to perform this correction, the delta visibilities generated by these sources need to be determined.

This computation is done simply by multiplying the Brightness Temperatures of each of these sources by the instrument forward model (G-Matrix). As for the Sun, since its precise Brightness Temperature is not known a priori, a self-estimation is performed – using the Calibrated Visibilities themselves and performing a Discrete Fourier Transform [3] over the precise coordinates of the Sun position. In alternative, an auxiliary data file containing the brightness

temperatures of the Sun can be used. The Moon is removed in the same way as the Sun.

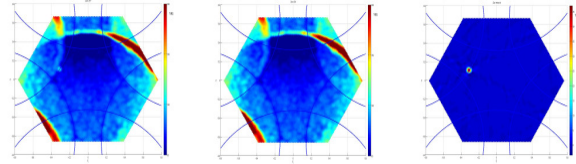


Figure 5. No Direct Sun removal (left), Direct Sun removed (center), image removed (right)

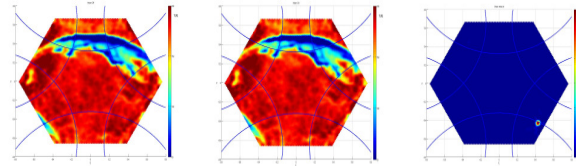


Figure 6. No Direct Moon removal (left), Direct Moon removed (center), image removed (right)

The Galaxy contribution to the scene can also be computed using the position, velocity and time (PVT) and attitude and angular velocities (AOCS) data from telemetry, to obtain the Earth-Sky limb, as well as an L-band Galaxy Brightness Temperature map to obtain the values over the 128x128 grid.

Sun-glint contribution to the scene can be computed using PVT and AOCS plus a bi-static scattering coefficients model [6] in order to obtain yet another Brightness Temperature distribution over the same 128x128 grid.

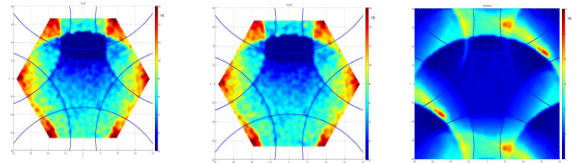


Figure 7. No Galaxy removal (left), Galaxy removed (center), image removed (right)

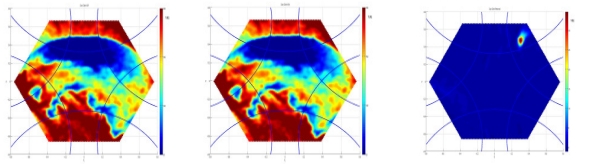


Figure 8. No Sun Glint removal (left), Sun Glint removed (center), image removed (right)

Figs. 5 to 8 present the tests done with real data for each of the algorithms described. Backlobes contribution removal is not shown since the effect was found to be below  $10^{-3}$  Kelvin in the AF-FOV.

### 3.1. Summary

This study shows that the removal of Direct Sun, the Moon and the backlobes contribution are performing according to the specifications. Thus, the usage of these algorithms has been recommended as baselines for operational processing.

Sun Glint removal, however, presented some artifacts near the Earth limb, as seen in Fig. 8, and its usage was not recommended for baseline processing. Further work will assess whether this algorithm is needed at Level 1 processing or whether the efforts should be put in Level 2.

## 4. INSTRUMENT PERFORMANCE ANALYSED WITH DEEP SKY OBSERVATIONS

To assess on the accuracy and performance of Dual and Full polarimetric modes several maneuvers have been performed during the Commissioning Phase of SMOS. The results presented in this section used two Flat Target Responses data sets acquired in January 2010 (19<sup>th</sup> and 21<sup>st</sup>) to derive all its conclusions. Data from 19<sup>th</sup> January was used as the target to be imaged and the maneuver of 21<sup>st</sup> January was used to derive the Flat Target Transformation.

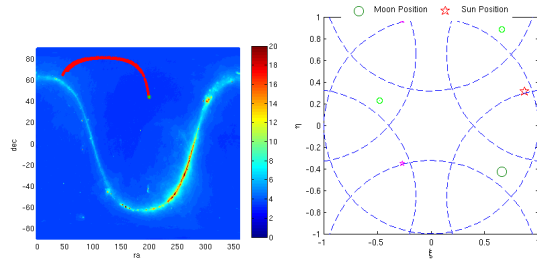


Figure 9. Trajectory for external manoeuvre of 19-Jan-2010 (left) and Sun and Moon Position during the FTR (right)

### 4.1. Accuracy

The accuracy has been defined as

$$Acc = \sqrt{\langle \bar{T}(\xi, \eta) \rangle^2 + \bar{\sigma}^2} \quad (1)$$

where  $\langle \bar{T}(\xi, \eta) \rangle$  is the average Time Averaged Temperature computed for a number of snapshots and  $\bar{\sigma}$  is its space standard deviation.

Applying the Sky Removal Algorithm and the Flat Target Transformation to the target image,  $\bar{T}(\xi, \eta)$  has been computed for over ~300 snapshots (Fig. 10) and from its statistics the final values for the MIRAS instrument accuracy were found, being presented in Tab. 1.

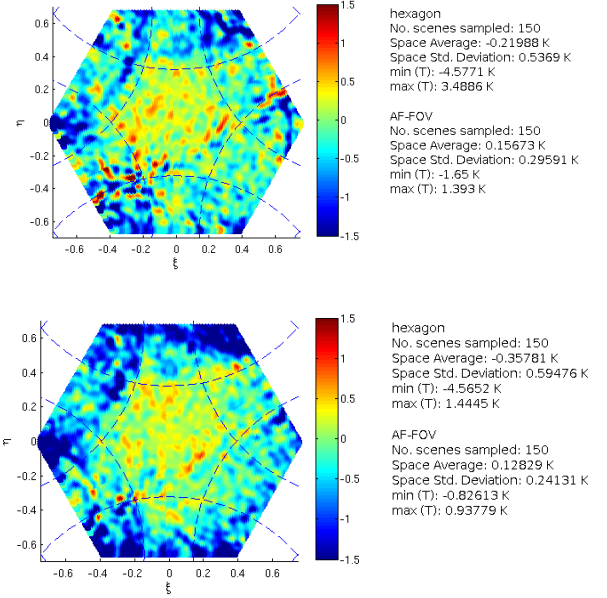


Figure 10. Time Averaged Temperature for Dual Pol observation of the Deep Sky used to compute the Accuracy (top: H-pol; bottom: V-pol)

### 4.2. Radiometric Sensitivity

The radiometric sensitivity is computed over N-snapshots using Eq. 2.

$$\bar{\sigma}(\xi, \eta) = \sqrt{\frac{1}{N} \left( \sum_{n=1}^N T_n(\xi, \eta)^2 \right) - \bar{T}(\xi, \eta)^2} \quad (2)$$

By defining the distance to boresight as

$$\rho^2 = \xi^2 + \eta^2 \quad (3)$$

and grouping the  $\rho$  points, the Radiometric Sensitivity is presented in Fig. 11 as a function of the distance to boresight. The red and blue points represent the observed values for the radiometric sensitivity, and the red and blue curves are computed as a least squares fit to

$$dT = a(1 - \rho^2)^{-3/2} + dT_o \quad (4)$$

where  $dT$  is the Radiometric Sensitivity in the  $(\xi, \eta)$  domain inside the Circle  $r = 0.3$ .

As expected, data from Pure Scenes in Full Pol follows the same distribution as the one from Dual Pol mode. The function in Eq. 4 has also been fit to H- and V-pol from Dual Polarimetric mode, as well as Re(HV) and Im(HV). The results obtained can be found in [5] and the values derived from the fit are very consistent within polarizations and polarimetric modes.

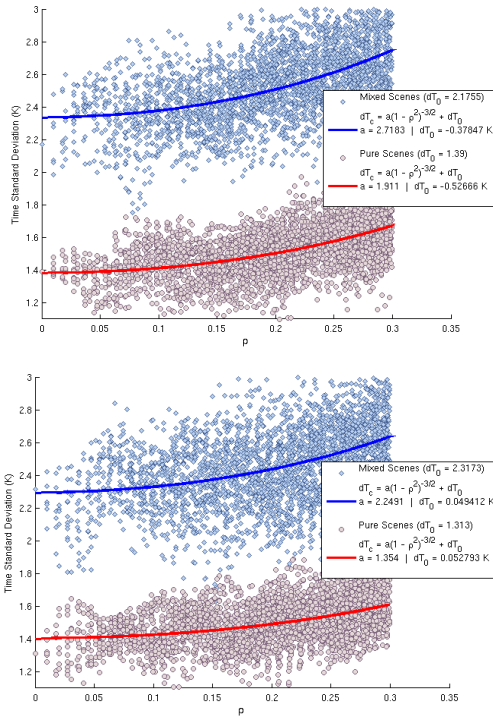


Figure 11. Radiometric Sensitivity as a function of distance to boresight in Full Polarisation for Pure and Mixed Scenes (top: H-pol; bottom: V-pol)

### 4.3. Summary

The analysis of MIRAS' performance has been summarized in Tab. 1, where the zones that have been represented are the hexagon, and the  $(\xi, \eta)$  Circle with  $r = 0.3$ . Other conclusions derived from the analysis of the Radiometric Sensitivity and Accuracy are presented in Section 5.

## 5. FINAL ASSESSMENT BETWEEN DUAL AND FULL POLARISATION DATA

The two modes available for SMOS (Dual and Full polarimetric modes) produce results very similar, but with small differences, both in their imaging results, as well as the performance parameters analysed. For example, Tab. 1 shows that the Radiometric Sensitivity exhibits some differences, which are within expectations, since the two modes use different strategies to acquire the data.

Table 1: Figures of merit for MIRAS' performance

Mode	Pol	Accuracy		Radiometric Sensitivity	
		Hexagon	Circle $r = 0.3$	$\bar{\sigma}(0,0)$	Circle $r = 0.3$
Dual	H	0.580	0.337	1.474	1.535
	V	0.694	0.279	1.436	1.527
	H	0.749	0.316	1.833	2.110
	V	0.777	0.291	1.887	2.051
Full	Re(HV)	0.435	0.312	1.926	2.037
	Im(HV)	0.367	0.251	1.961	2.047
	Pure H	0.762	0.339	1.390	1.524
	Pure V	0.763	0.299	1.313	1.505
	Mixed H	0.827	0.384	2.176	2.538
	Mixed V	0.865	0.373	2.317	2.317

### 5.1. Imaging Results

A comparison of the Time Averaged Temperature maps obtained from the same target, but acquired in different polarimetric modes (Fig. 12), shows that there is no structure in the differences patterns: i.e. any existing difference is random and is not due to the instrument mode. Furthermore, the average value of the differences is very small. Fig. 12 represents the worse case of these differences.

Furthermore, when analyzing the Time Averaged Temperature for all polarizations of the two polarimetric modes (H-, V-, Re(HV) and Im(HV) pol), it has been observed that the space standard deviation is roughly the same for dual and full pol mode, in the order of 0.3 K.

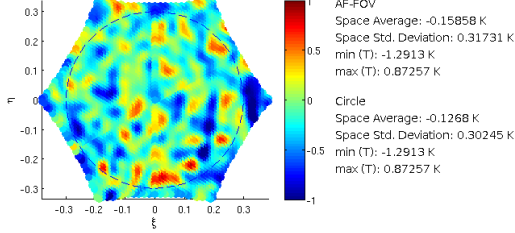


Figure 12. Difference between Time Averaged Scenes for Observed Sky, Full - Dual, in the AF-FOV in H-pol

## 5.2. Instrument Performance

In terms of Accuracy, the differences between Dual and Full polarization within the  $(\xi, \eta)$  Circle with  $r < 0.3$  (Tab 1) show that the accuracy degrades by  $\sim 6\%$  and  $4\%$  in H- and V-pol, respectively.

Another analysis has been performed to assess the differences on Radiometric Sensitivity from Dual and Full polarization. Without making a distinction between Pure and Mixed scenes in the full polarimetric mode, the comparison between the Radiometric Sensitivity is shown in Fig. 13. The degradation of the sensitivity in the AF-FOV is  $\sim 0.5$  K, corresponding to  $\sim 37\%$  and  $34\%$  for H- and V-pol. There are no privileged zones that get more affected by the Full polarimetric mode.

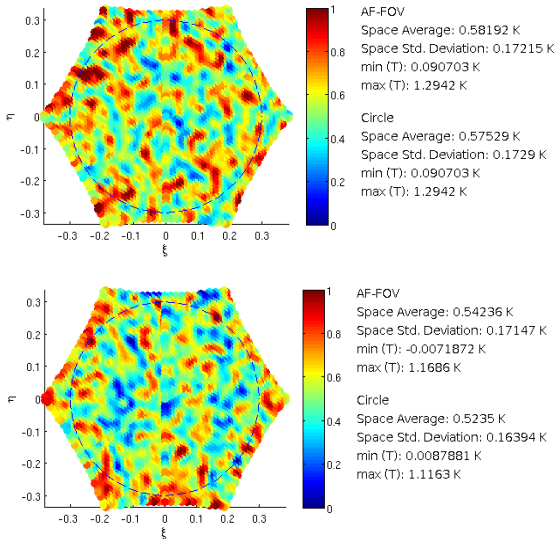


Figure 13: Differences in Radiometric Sensitivity, Full - Dual, in the AF-FOV (top: H-pol, bottom: V-pol)

## 5.3. Noise Ratios

Using empirical data for the Radiometric Sensitivity in the Circle  $r = 0.3$  taken from Tab.1, the ratios

- between Full Polarisation and Dual Polarisation Scenes (this is computed taking the average of H- and V-pol scenes); and
- between Mixed Scenes and Pure Scenes from Full Polarimetric Mode (for this computation the value for the Mixed Scenes is the average of H- and V-pol Mixed Scenes. Similarly, the value for Pure Scenes is the average of H- and V-pol Pure Scenes)

can be computed and are summarized in Tab.2, column one.

The noise between Dual and Full polarimetric mode is quantified by the theoretical ratio of noise amplitudes,  $\alpha$ , as shown in Eq. 5 [11].

$$\alpha_{(1,2)}^{(t)} = \sqrt{\frac{\tau_2^{(t)}}{\tau_1^{(t)}}} \quad (5)$$

Eq. 5 is written in a general form, where the superscript  $(t)$  is used to identify the theoretical values for the integration time,  $t$ , of the modes indexed by the subscripts  $(1)$  and  $(2)$ . Taking

- 1.2 seconds for Dual Polarisation Scenes and Pure Scenes;
- 0.4 seconds for Mixed Scenes; and
- 0.6 seconds for Full Polarisation Scenes in HV (This value corresponds to the average effective integration time when pure and mixed scenes are combined together)

the theoretical ratios of noise are computed and presented in Tab. 2, second column.

Table 2: Noise Ratios

	Empirical Ratio	Theoretical Ratio
(Full, Dual)	1.36	1.41
(Mixed, Pure)	1.59	1.73

As can be seen, the observed ratios are always better than the theoretical expectations. This evidence is justified with the fact that the theoretical ratios have

been estimated without taking into account the higher degree of baseline redundancy contained in the Mixed scenes from Full Pol data.

#### 5.4. Summary

The results presented in this section show that Full Pol mode, when compared against Dual Pol mode, behaves according to the expectations, and sometimes even surpassing them. The final decision on the polarization mode of the MIRAS instrument was taken at the end of the SMOS Commissioning Phase, based on the inputs presented in the previous sections. Since the degradation is compliant with the requirements and given the fact that the Full Polarimetric mode contains more information (namely HV-pol information), this was the selected mode for the Operational Phase of SMOS.

#### 6. CONCLUSIONS

The LIPP has played a key role during the SMOS Commissioning Phase, since it was the software used to give feedback to the Management team. The recommendations from Level 1 teams on the operational mode for SMOS, as well as the LO frequency, were given based on data processed with LIPP.

Results obtained with LIPP also forced a revisit on the Full Polarimetric theory. The integration time for scenes acquired in this mode had to be corrected.

During the Operational Phase of SMOS, LIPP will continue to be the testing environment to implement new algorithms and improve the existing ones.

#### 7. REFERENCES

1. Barbosa, J. & Gutierrez, A. (2010), SMOS L1 Processor L0 to L1a Data Processing Model, SMOS Project Documentation
2. Brown, M. (2007). SMOS Calibration, in IEEE IEEE Transactions on Geoscience and Remote Sensing, XX SMOS Special Issue.
3. Camps, A., Vall-llossera, M, Duffo, N., Zapata, M, Corbella, I., Torres, F. & Barrena, V. (2004), Sun Effects in 2D Aperture Synthesis Radiometry Imaging and their cancelation, in IEEE IEEE Transactions on Geoscience and Remote Sensing, 42 (6) 1161-1167. ISSN: 0196-2892
4. Castro, R. & Martin-Porqueras, F. (2010), SMOS L1 Flat Target Validation, SMOS Project Documentation
5. Castro, R. (2010), SMOS L1PP MIRAS Performance for Dual and Full, SMOS Project Documentation
6. Castro, R., Oliva, R. & Martin-Porqueras, F. (2010), SMOS L1 G and J+ Matrices Validation, SMOS Project Documentation
7. Freitas, J, Correia, J. & Catarino, N. (2010), SMOS L1 Processor L1a to L1b Data Processing Model, SMOS Project Documentation
8. Gutierrez, A. & Castro, R. (2010), SMOS L1 Processor L1c Data Processing Model, SMOS Project Documentation
9. Martin-Neira, M. & Brown, M. (2010). In-Orbit Commissioning High Level Plan, ESTEC publication.
10. Martin-Neira, M. (2007), SMOS FTT, in IEEE Transactions on Geoscience and Remote Sensing, XX SMOS Special Issue.
11. Martin-Neira, M. (2010), On Noise Ratio Dual vs Full, ESTEC publication.
12. Oliva, R. (2010), Local Oscillator Decimation Study, ESAC Publication